NJC

ROYAL SOCIETY OF CHEMISTRY

PAPER

View Article Online
View Journal | View Issue

Cite this: *New J. Chem.*, 2026, **50**, 5104

A sustainable one-pot synthesis of chiral carbon dots using response surface methodology: elucidating the mechanistic pathways through biological responses

Arezoo Setayesh,[ac] Laura Domínguez Mercado,[a] Adryanne Clermont-Paquette,[abc] Brandon L. Findlay[ab] and Rafik Naccache *[ac]

Chirality is fundamental to nature, and the distinct interactions of optically active molecules in a chiral environment are crucial for a multitude of applications. Chiral nanomaterials such as carbon dots (CDots) have attracted considerable attention due to their synthetic tunability. This tunability can be easily customized using single-step microwave-assisted techniques from relatively inexpensive and versatile molecules. Through adjusting reaction parameters, it is possible to transfer chiroptical properties from precursors to CDots while maintaining their active structure. While tunability can be achieved through bottom-up synthesis approaches, it is often time-consuming and requires multiple experiments. Herein, chiral CDots were synthesized from L-/D-proline as the chiral precursor and citric acid as the co-carbon source *via* a single-step microwave-assisted reaction. The duration of the synthesis, the molar ratio of chiral precursor, and the temperature of the reaction were optimized using response surface methodology-Box–Behnken design. Through active structure preservation, we were able to preserve chiral centers on the surface of CDots. CDots prepared at a temperature that preserved chirality inhibited the growth of Gram-negative and Gram-positive bacteria more efficiently than an achiral variant. Further evaluation of the mechanism of action for CDots suggested their antibiotic activities to be bactericidal, resembling the activity of polymyxin B in our study. Our findings shed light on the capacity of biological systems to discriminate between chiral and non-chiral-based CDots and can inspire new ideas in antibiotic and smart surface research.

Received 14th November 2025,
Accepted 18th February 2026

DOI: 10.1039/d5nj04463d

rsc.li/njc

Introduction

Chirality plays a crucial role in the binding of biologically active molecules to their targets, particularly in the case of antibacterial agents and their interactions with cellular targets. The advent of nanotechnology has brought the concept of incorporating chirality at the nanoscale to the forefront, as evidenced by its reported use in various forms, including nano-assemblies,[1] nanocrystals,[2] and semiconductor quantum dots for a range of biological applications[3–5] sensing systems[6,7] and catalysis.[8] Of particular interest for chirality at the nanoscale are carbon dots (CDots), which were introduced to the field in 2004 by Xu *et al.*[9] CDots are photoluminescent carbon-based nanoparticles with tunable properties.[10–12] Tunability of CDots could be defined as chemical, optical, or a combination of both, depending on the chemical precursors and the conditions upon which the synthesis was performed. The vast range of chemical precursors that can be used to make CDots has spurred numerous investigations into potential biosensing applications,[13,14] cancer therapy,[15–17] and antimicrobial systems.[18,19] Recently, a novel approach to creating chiral CDots has emerged, whereby chiral molecular precursors are used to generate CDots with inherent chiral properties under hydrothermal conditions, without requiring additional post-synthesis modifications.[13,20–22] This process occurs in the bottom-up synthesis of CDots, where reaction parameters are controlled to preserve or transform some of the properties of precursors into CDots, known as active structure preservation in the literature.[23–26]

As this area of research progressed and more studies were conducted on chiral CDots, the transfer, or induction of chirality from amino acids gained significant attention. Amino acids are a relatively inexpensive class of compounds that exhibit a broad range of chemical and physical characteristics,

[a] *Department of Chemistry and Biochemistry and Center for NanoScience Research, Concordia University, Montreal, QC, H4B 1R6, Canada. E-mail: rafik.naccache@concordia.ca*
[b] *Department of Biology and the Centre for Microscopy and Cellular Imaging, Concordia University, Montreal, QC, H4B 1R6, Canada*
[c] *Quebec Centre for Advanced Materials, Department of Chemistry and Biochemistry, Concordia University, Montreal, QC, H4B 1R6, Canada*

including hydrophobicity, hydrophilicity, and aromatic functional groups.[27–30] Given their fundamental role as the building blocks of proteins and their capacity to act as signalling molecules in intercellular communication, amino acids have emerged as promising chiral precursors for the synthesis of CDots in biological systems. Previous studies reported successful synthesis of chiral CDots from amino acids such as glutamic acid and methionine,[31] lysine,[32] alanine and aspartic acid,[33] tyrosine,[34] and tryptophan.[35] However, limited studies have investigated the antibacterial effect of amino acid-based CDots.[28] Additionally, the extent to which the chiroptical properties of amino acids are retained and how they could potentially influence their antibacterial properties remains an area of limited investigation.

Proline is a nonpolar amino acid with a unique cyclic structure, distinguishing it from other proteinogenic amino acids commonly used as precursors, such as L-cysteine.[36] Several studies have demonstrated that proline-rich peptides possess substantial antibacterial activity against a variety of bacterial strains.[37–41]

In this study, we synthesized chiral CDots from the mixture of L-/D-proline and citric acid, *via* a single-step microwave-assisted reaction. To understand the effect of residual chiral centers on the surface of the CDots and investigate their potential enantiomer selectivity, we attempted to maximize the chiral signal of the synthesized CDots. Response surface methodology (RSM) was used for the first time to elucidate the reaction conditions (temperature, time, and molar ratio of precursors) that would result in the maximum preservation of chirality in CDots. Behnken design (BBD) was selected as the experimental design in RSM and as the main strategy to study the reaction parameters to minimize the number of experimental runs while respecting their synergistic effect on the chiral signal. Finally, to explore the capacity of biological systems to differentiate between chiral and non-chiral CDots and to investigate the potential antibacterial properties of chiral CDots, we assessed the impact of these materials on various bacterial strains. Minimum inhibitory concentration (MIC) and time-kill assays were performed on chiral CDots synthesized from L- and D-proline and compared to controls of CDots bearing no chiral signal, but with the same chemical composition. Our findings have the potential to open new avenues for research and applications centered on the chiroptical properties of CDots.

Experimental and methods

Materials

All reagents and solvents were used as is without further purification. L-Proline (>98%) and citric acid anhydrous (>99.5%) were purchased from Sigma Aldrich. D-Proline (>98%) was purchased from TCI.

Experimental design and numerical optimization

CDots were synthesized *via* a microwave-assisted reaction. The impact of three selected factors, namely reaction time, temperature, and molar ratio of proline to CA on the magnitude of chiral signal was investigated *via* a Box–Behnken design (BBD). Table 1 shows the high and low values (levels) for each independent factor along with the center (medium) levels used to generate the randomized sequence of experiments in BBD. Accordingly, the independent response (Y) was set as the integration of chiral signal measured in the circular dichroism spectra within the range of 180–220 nm for all samples. The chemical similarity of L-proline and D-proline prompted the optimization of chiral CDot synthesis exclusively for the L-enantiomer, which was subsequently designated as L-Pro.CA CDots. However, the optimum condition was later expanded to the synthesis of D-Pro.CA CDots to assess and evaluate enantioselectivity and antibacterial properties of both enantiomers.

Table 1 The independent factors for the optimization of chiral response for L-pro.CA CDots

Independent factors	Low level (−1)	Center point (0)	High level (+1)
(X_1) time	10 min	17.5 min	25 min
(X_2) temperature	160 °C	175 °C	190 °C
(X_3) molar ratio	3 : 1	5 : 1	7 : 1

Synthesis of CDots

As shown in Scheme 1, for each experimental run, a mixture of 0.5 M citric acid (CA) was prepared in 10 mL Milli-Q water with the corresponding molar ratio of L-proline, according to the experimental data set in Table S1, and sonicated to form a homogeneous solution. Subsequently, the solution was transferred into 35 mL CEM microwave vials and heated at the corresponding time and temperature in the reactor indicated by the data set. The crude product from the reaction was purified from the unreacted compounds *via* dialysis (Spectra/Por®6 RC – Spectrum Laboratories) for 2–3 days and dried in the oven to remove the solvent. The dried powder was further subjected to solid–liquid extraction with a mixture of ethanol : acetone prepared at a ratio of 2 : 10, centrifuged at 10 000*g* for 10 minutes and dried overnight to remove solvent residue. The pellets were further collected and used for characterization of the L-Pro.CA CDots.

Physicochemical characterization of CDots

To obtain information about the overall morphology and the size distribution of CDots, transmission electron microscopy (TEM) was used. Dried CDots were dispersed in isopropanol/Milli-Q water (50 : 50, v/v) at a concentration of 1 mg mL^{-1} and sonicated for 10–15 seconds. The solution was applied dropwise on the 300 Mesh copper (Cu-300HD) coated with holey/thin carbon films (Pacific Grid Tech) operating at 5 kV. The UV-Vis absorption spectra were obtained using a Cary 5 series UV-Vis-NIR Spectrophotometer (Agilent Technologies) in the spectra range of 200–800 nm. A 1 cm quartz cuvette was used with wavelength changeover at 350 nm and 5 nm bandwidth.

The fluorescence emission was recorded using a Cary Eclipse fluorescence spectrophotometer (Agilent Technologies). The concentration for CDots was adjusted to OD < 0.1 to avoid inner filter effects. CDots were excited from λ_{250} to λ_{550} nm with 50 nm intervals. The excitation and emission slits were both set to 5 nm, and all data was processed using Agilent Cary Eclipse

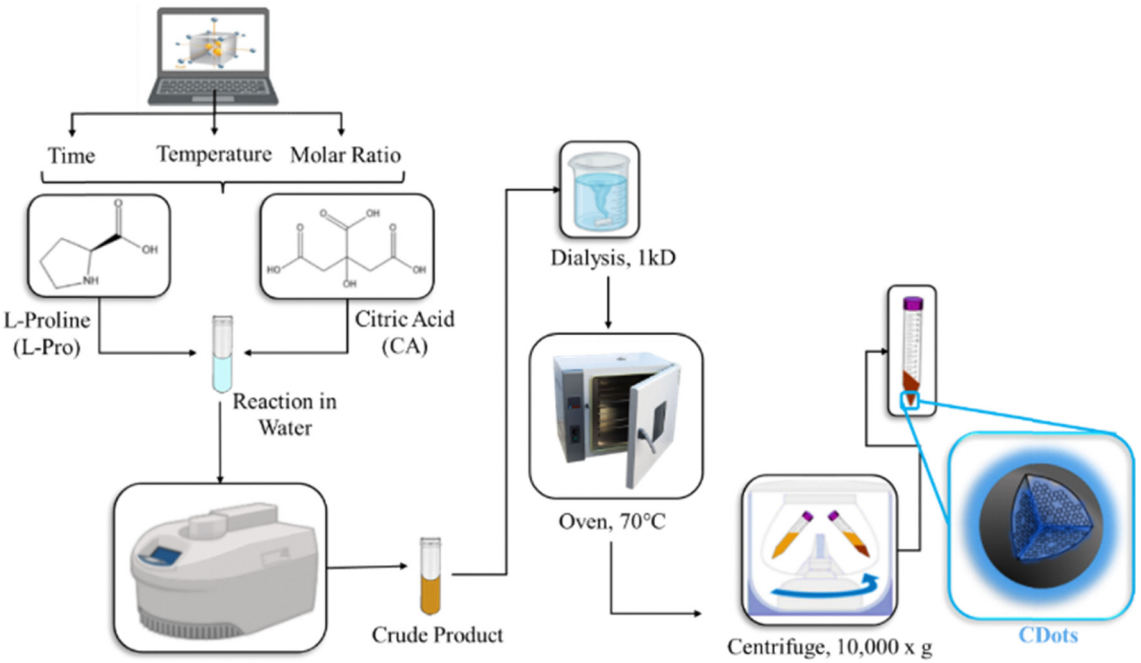

Scheme 1 Optimization and synthesis of L-Pro.CA CDots *via* microwave reactor.

software package. The circular dichroism (CD) spectra were obtained using a JASCO J-815 spectropolarimeter in the spectra range of 180–400 nm and in 3 accumulations. The scans were continued with the speed of 50 nm min^{-1} using a 1 mm quartz cuvette. The data was analyzed using Spectra Manager II software. To investigate the surface chemistry of CDots, the Fourier transform infrared spectra (FT-IR) were collected using a Thermo Scientific Nicolet iS5 equipped with an iD5 attenuated total reflectance (ATR) accessory. The spectra were obtained using 64 scans with resolution of 0.4 cm^{-1}, a gain of 1, an optical velocity of 0.4747 and an aperture setting of 100. The Omnic 9 software was used to process the data. The X-ray photoelectron spectroscopy (XPS) spectra were collected using a Thermo-Scientific K-alpha X-ray photoelectron spectrometer. Each analysis was performed on three different spots on the sample, in triplicates, with 5 runs for each scan. The average for high resolution and survey was plotted. To assess the crystallinity and structure of CDots, X-ray powder diffraction (PXRD) technique was used. The PXRD data were conducted on a Bruker D8 advance diffractometer equipped with a LYNXEYE linear position sensitive detector (Bruker AXS, Madison, WI). Neat samples were smeared directly onto the silicon wafer of a proprietary low-zero background sample holder and data was collected in the 2θ-range of 10–90° in increments of 0.02°. To evaluate the thermal stability of the samples, thermogravimetric analysis (TGA) was carried out using a TGA Q500 analyzer. Samples were heated from 25 to 1000 °C at a rate of 5 °C min^{-1} under an Argon atmosphere with a flow rate of 90 mL min^{-1}.

Antibacterial activity of chiral CDots

Antimicrobial susceptibility against the CDots was measured by broth microdilution to determine the MIC of different Gram-negative and Gram-positive bacteria as per CLSI guidelines.[42] In brief, 96-well polypropylene plates were used to create a concentration gradient with increasing two-fold concentrations of the compounds tested. The bacterial strains tested were incubated overnight and diluted to the turbidity of a 0.5 McFarland standard, then further diluted 1 : 100 in MHB2 (Cation-adjusted Muller Hinton Broth). To determine the time-kill kinetics, exponentially growing *E. coli* ATCC 25922 cells (OD ≈ 0.364, diluted to a final OD ≈ 0.1821) were treated with CDots and various established antibacterial compounds with known mechanisms of action. The cells were incubated at 37 °C with shaking, and the absorbance was recorded at 595 nm every 5 minutes using a TECAN Magellan plate reader.

Results and discussion

Synthesis and optimization of CDots

Bottom-up approaches using small organic precursors to synthesize CDots have been employed extensively through microwave-assisted techniques to preserve some of the properties of precursors in CDots.[43] Citric acid, as a tricarboxylic acid, is quite prominent in bottom-up approaches of CDot preparation.[44–46] Enriching the surface of citric acid-based CDots with chiral properties requires precise tailoring of the conditions that favor preservation of the chiral centers during the reaction. It has also been demonstrated that the provision of heteroatoms through passivation represents a viable strategy for enhancing the reaction yield, a challenge that has been widely acknowledged in producing CDots.[47] Hence, L-/D-proline, a chiral molecule, can serve not only as a chiral precursor, but also as a passivating agent to effectively enhance the reaction yield of CDots.

In this study, response surface methodology utilizing BBD was employed to model and optimize the reaction conditions. The parameters of time, temperature, and molar ratio of L-proline to CA were systematically varied to determine and model the reaction conditions. Table S1 displays the results of the seventeen randomized experimental runs conducted using the BBD matrix with the corresponding integration of the chiral signal for the synthesized CDots. Lower chiral responses were observed at higher temperatures that correspond to elevated decomposition of the reactants, especially the chiral precursor and its chiral centers. Run 15 shows the lowest value for the response (159.9-integrated area) at 190 °C, 25 min, and 5 : 1 proline : CA ratio. Conversely, run 1 shows the highest response (547.6-integrated area) at 160 °C, 17.5 min, and 3 : 1 proline : CA ratio. Also, the chiral signal decreases as the ratio of chiral precursor increases from 3 : 1 to 7 : 1 which could indicate that the formation of chiral CDots is not necessarily following an enhancement by increasing the amount of enantiomer in the reaction. Instead, only limited regions, likely on the surface, can contribute to the observed chiral response and may reach saturation after a certain concentration of the enantiomer is achieved. To further investigate this observation, an exploration was conducted into the impact of molar ratios below 3 : 1 of proline : CA (not depicted). It was observed that no product was obtained at lower ratios. This absence of product suggests a significantly reduced reaction efficacy at lower quantities of carboxylic acid and amino groups, a phenomenon consistent with prior reports.[47]

Table S2 shows the result for the sequential model sum of squares according to the experimental runs. The quadratic model used for this experiment provides a higher order polynomial compared to a linear model, and it is not aliased like a cubic model. Also, the *P*-value for the quadratic model (0.0059) is less than 0.05, which is within the significant range of this study. The adequacy of the quadratic model was evaluated with ANOVA as presented in Table S3. The significance of the fitness of the model was evaluated by the very small *P*-value (<0.0001) and the insignificance of the lack-of-fit (0.7373). Also, the *P*-value for each variable and its interactions should be significant to be included in the final model.

The final form of the quadratic coded model based on the estimation for coefficients of each significant term in the ANOVA table is displayed as eqn (1):

$$Y = 5.99 - 0.15X_1 - 0.29X_2 - 0.14X_3 - 0.21X_1X_3 + 0.13X_1X_2 - 0.11{X_1}^2 - 0.10{X_2}^2 \quad (1)$$

where X_1, X_2, and X_3 correspond to time, temperature, and molar ratio of L-proline:CA and the interactions between the main factors are represented by X_1X_3 and X_1X_2. Additionally, ${X_1}^2$ and ${X_2}^2$ represent second-order terms for time and temperature, respectively. The coefficient for X_2 (0.29) holds the highest value among the terms within the model. This outcome signifies that the most substantial influence among the factors is attributed to the fluctuations in temperature. This is in accordance with previous studies showing the significance of temperature in the overall formation of CDots in addition to their chirality.[28,48–50] The coefficients signifying the interactions involving time and temperature (X_1X_2), as well as the interaction term for time and molar ratio (X_1X_3), within the model, are 0.13 and 0.21, respectively. Notably, these values closely resemble the coefficients assigned to the primary factors, namely time X_1 (0.15) and molar ratio X_3 (0.14). This alignment implies that the combined variations of these two parameters hold equivalent significance to the main factors in influencing the residual chiral response. Moreover, the values for the coefficient of determination (*R*-squared = 0.98, adj. *R*-squared = 0.96, and pred. *R*-squared = 0.91) suggest a strong agreement between the quadratic model and the experimental data. The reliability of the model is also demonstrated in Fig. 1A, as the actual data is approximately in accordance with the straight line showing the predicted amounts based on the estimation of the quadratic model. This finding further affirms the satisfactory nature of the residuals in the experimental data, thereby validating the ability of the model to fit the data. Furthermore, Fig. 1B depicts the residuals plotted against the ascending predicted response values, which demonstrates a random distribution within an acceptable range. The internally studentized residuals possess the ability to measure the magnitude of residuals in terms of standard deviation units, thereby facilitating their application in detecting outliers. Specifically, an observation that exhibits an internally studentized residual exceeding 3 (in absolute value) is typically identified as an outlier.

3D plots were also generated to better demonstrate of the relationship between the variables and the response. The effect of L-Pro : CA molar ratio and time on the chiral integration is shown in Fig. 1C, which displays maximum chiral responses at a lower molar ratio with a decrease in the response as the molar ratio increases. The bottom-up synthesis of CDots is based on the general assumption that prolonging the reaction will result in greater consumption of the reactants due to polymerization, which leads to the formation of well-hybridized CDots.[28,51]

Accordingly, the chiral response should have also decreased as the decomposition of the chiral centers takes place.

Nevertheless, the variation in time appears to follow a curved pattern, whereby the chiral response initially increases with time. However, shortly after reaching the midpoint at approximately 17.5 minutes, it begins to decrease.

This observation suggests that the surface of CDots may have a limited number of interaction sites available for the attachment of residual chiral centers. Moreover, increasing the concentration of CDots could lead to steric hindrance by the bulky structure, thereby potentially impeding the chiral signal. Fig. 1D shows a similar trend for temperature, with an initial increase in chiral response observed up to approximately 167 °C, followed by a subsequent decrease as the temperature reaches 190 °C. To further clarify this phenomenon, experiments were conducted at lower temperatures below 160 °C; however, no formation of CDots was observed at temperatures below 160 °C, even with 30-minute exposure time to microwave irradiation. Utilizing a shorter exposure time and lower reaction temperature to synthesize chiral CDots could confer a advantage to this system in terms of energy efficiency.

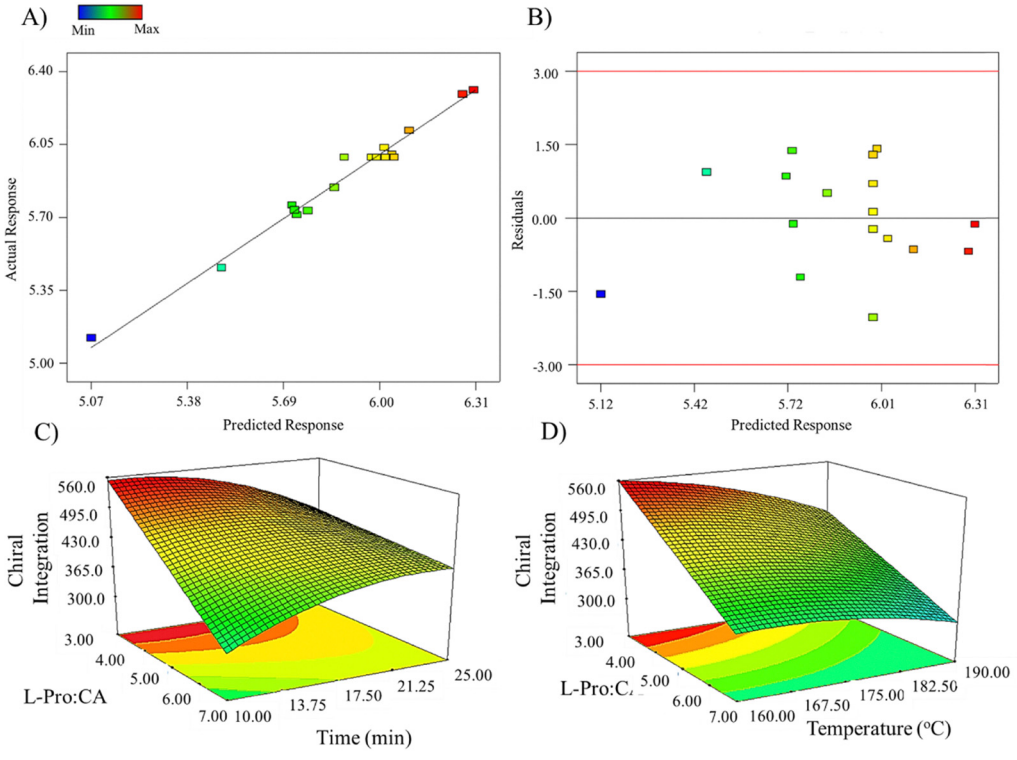

E)

Experiment	X_1 (Time/min)	X_2 (Temperature/°C)	X_3 (Molar ratio)	Y_{Ex} (Experimental)	Y_M (Model)
1	10	160	3	539.4	549.9
2	15	160	4	493.4	511.3
3	20	170	3	466.8	457.6
4	13	163	3	550.2	552.0
5	18	175	4	411.7	420.7

Fig. 1 The graph of the actual response values for the chiral integration *versus* the predicted response values (A); the plot of the residuals *versus* the ascending predicted response values with the random scatter of the plot with no specific trend (B); 3D surface plots from optimization of chiral response using BBD showing a functional relationship between the dependent response (chiral integration) and independent variables. L-Pro:CA and time (C) and L-Pro:CA and temperature (D); results of confirmation experiments for L-Pro.CA CDots (E). The conditions were used to conduct confirmation experiments and to compare the experimental responses (Y_{Ex}) with the predicted model responses (Y_M).

Therefore, to further characterize the samples, several conditions were selected as outlined in Fig. 1E to perform validation experiments and compare the corresponding responses with the estimated responses of the model. Based on the findings presented in Fig. 1E, all experimental values exhibited a high degree of agreement with the estimated values derived from the model. This consistency between experimental and modelled values serves as a testament to the reliability of the model. To continue with the maximum chiral response observed in the study, additional characterization was performed on the sample from Experiment 4. The reaction yield for this particular sample was determined through the calculation of three independent replicates based on the mass of the precursors and the products, with a value of 34%. Given the context of prior research, microwave-assisted reactions usually yield CDots within the range of 10–30%.[52] Consequently, the decision was made to proceed with this particular sample, considering its alignment with the expected yield range.

Characterization of CDots

Chiral CDots (L-Pro.CA CDots) were synthesized through a microwave-assisted synthesis at the selected condition (163 °C, 3 : 1 molar ratio, 13 min). Following each reaction, extensive purification was carried out to ensure removal of unreacted

precursors. This was achieved through dialysis and solid–liquid extraction. The size and morphology of CDots were explored through transmission electron microscopy (TEM). As shown in Fig. 2A, CDots appeared quasi-spherical with an average size of 16.5 ± 3.5 nm and a Gaussian size distribution in the range of 8–28 nm consistent with findings from prior studies utilizing amino acids in combination with citric acid as precursors.[25] The optical properties of L-Pro.CA CDots along with the precursors were characterized by UV-Visible and fluorescence spectroscopies (Fig. 2B). The appearance of the absorbance at ~250 nm is the characteristic of the π → π* transition attributed to the aromatic sp2 domains, which coincides with the region for the absorbance of the precursors. Additionally, the absorbance at ~350 nm in the UV-Vis spectra for CDots is often ascribed to a transition that arises due to the combination effect of the increase in O and N-doping of the structure. Furthermore, as depicted in the inset of Fig. 2B, the dispersion of chiral CDots in water showed a blue fluorescence with the maximum emission observed at 420 nm following excitation at 350 nm. We note that the precursors have no significant absorbance or fluorescence under these conditions.

In order to study the chemical composition of CDots, Fourier transform infrared (FTIR) spectroscopy and X-ray photoelectron spectroscopies (XPS) were used. Fig. 2C shows the FTIR spectra for the precursors (L-proline and CA) as well as the L-pro.CA CDots. The overall vibration profile of CDots exhibits major differences relative to the precursors. A notable difference is the broad band at 2500–3450 cm^{-1} observed for CDots, which is attributed to the O–H stretching of carboxylic acid and other oxygenated groups. The two distinct bands also present in

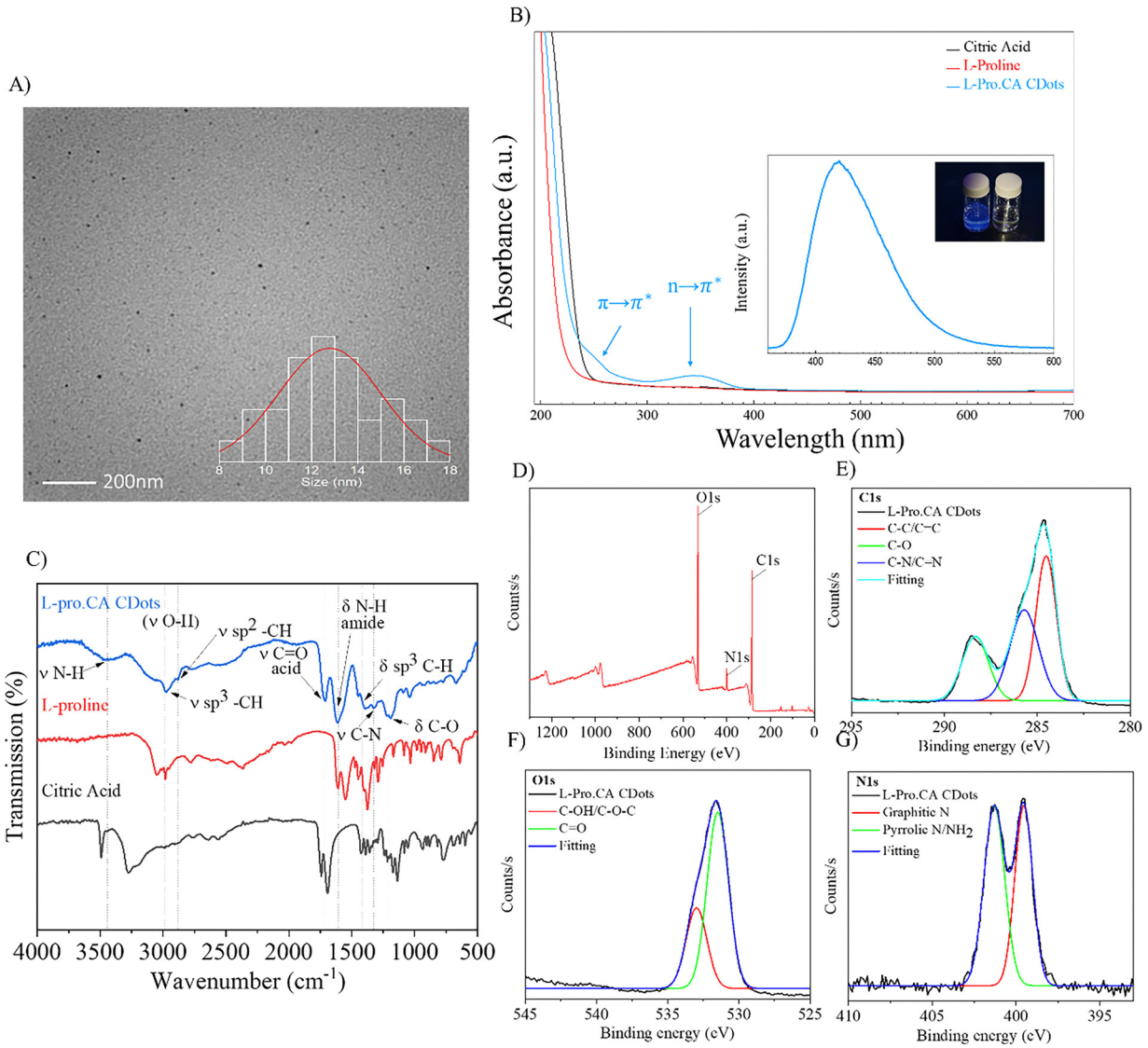

Fig. 2 Characterization of L-Pro.CA CDots. TEM images of L-Pro.CA CDots with an average dimension of 16.5 ± 3.5 nm (A). The UV-Vis spectra of L-Pro.CA CDots with two distinct peaks corresponding to the and transitions; the inset displays the fluorescence spectra of L-Pro.CA CDots when excited using λ = 350 nm showcasing a blue emission peak centered at 420 nm (B). FTIR spectra of L-pro.CA CDots and the precursors (C). Survey XPS scan of L-Pro.CA CDots illustrating the prominent elements in the structure (D). High resolution XPS scan for C1s (E), O1s (F), and N1s (G).

the spectra of CDots at 1612 cm^{-1} and 1705 cm^{-1}, along with the band at 1200 cm^{-1}, are attributed to N–H bending of amides, C═O stretching of carboxylic acids, and C–O stretching of acyl groups, respectively. In addition, sp^3 C–H stretching and bending at 3000 cm^{-1} and 1400 cm^{-1}, with the sp^2 C–H stretching at 2870 cm^{-1} confirms earlier studies on the sp^2–sp^3 nature of CDs prepared from citric acid as the precursor.[28,53]

XPS analysis was used to further expand our investigation of the surface composition of CDots. Fig. 2D shows the survey scan for L-Pro.CA CDots with prominent peaks at 530, 400, and 285 eV ascribed to the binding energies of O1s, N1s and C1s, respectively. Deconvolution of the high-resolution scan of C1s (Fig. 2E) showed binding energies at 288.3, 285.6, and 284.5 eV that can be attributed to C–O, C–N/C═N, and C–C/C═C. Furthermore, in the high-resolution scan of the O1s (Fig. 2F), two dominant peaks are evident at 533, and 531.4 eV corresponding to C–OH/C–O–C and C═O. Notably, the high-resolution N1s spectrum (Fig. 2G) reveals the presence of pyrrolic N/NH_2 and graphitic N, exhibiting distinct peaks at 401.3 eV and 399.5 eV, respectively. These results are also in accordance with the previous studies on passivated citric acid-based CDots.[51,54]

Following the chemical analysis, circular dichroism measurements were conducted on both the precursors and CDots to examine their differential absorbance of circularly polarized light. Circular dichroism occurs when the left-handed and right-handed circularly polarized absorbances are different, giving a positive or negative signal in the spectra. Proline exhibits a coupled oscillator circular dichroism (CD), also known as an exciton couplet, when the electric dipole transition moments of two chromophores within the structure are coupled together.[55] As shown in Fig. 3A, the positive cotton effect (CE) observed for L-proline was diminished to a single negative absorbance for the L-Pro.CA CDots. This further confirms the formation of a new structure that could be the result of transforming some of the chromophores and their incorporation into the hybridized CDot system. The impact of concentration of the chiral precursor (L-proline) and L-Pro.CA CDots on the CD spectra was also evaluated.

Fig. 3B illustrates the CD spectra of L-proline exhibiting an intensity-dependent pattern based on the concentration of the amino acid. As the concentration changes from 10 mg mL^{-1} to 0.08 mg mL^{-1}, a decrease in intensity occurs with no significant alteration or shift in the profile. This further confirms that the exciton couplet of L-proline does not follow a concentration-dependent pattern in the operating concentration but rather experiences a steady decrease in its signal. A comparable pattern is also observed in L-Pro.CA CDots with the variation of concentration from 1 mg mL^{-1} to 0.1 mg mL^{-1}, showing a decline in the CD signal until it completely vanishes. The observed effect can be attributed to the Beer–Lambert law in absorption techniques, which establishes a correlation between sample absorption and its concentration. Nonetheless, the CD spectra of L-Pro.CA CDots, as illustrated in Fig. 3C, exhibit a marked increase in absorbance, along with a noisy profile, at concentrations above 5 mg mL^{-1}.

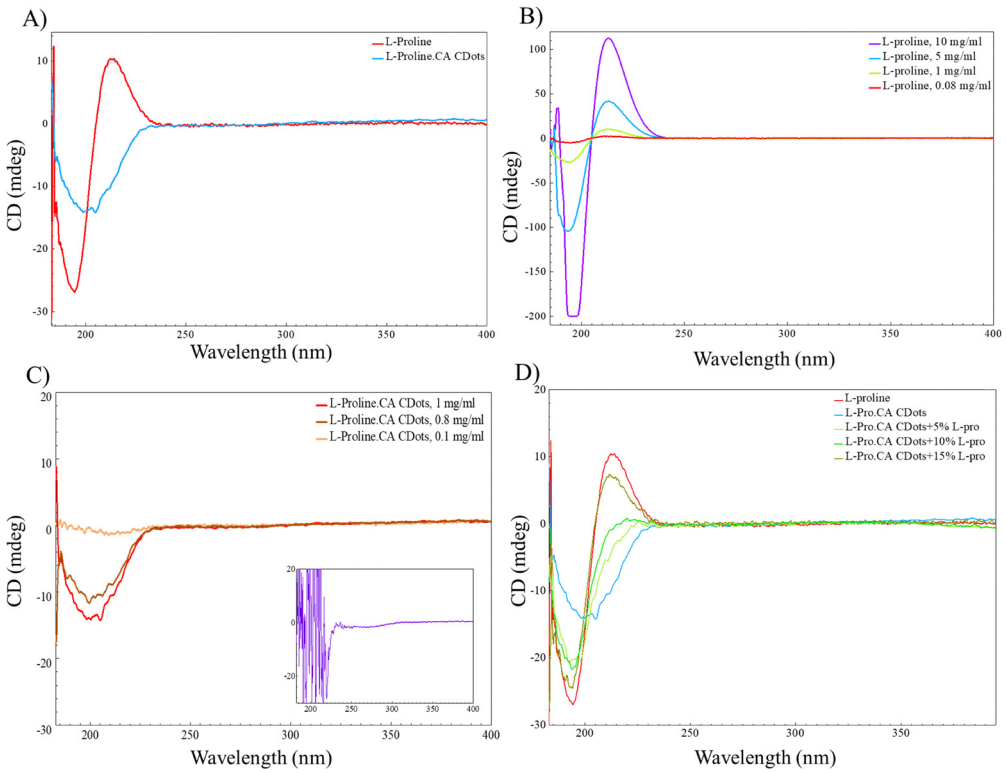

Fig. 3 Circular dichroism (CD) spectra of L-Pro.CA CDots and L-proline (A). L-proline at varying concentrations (B). L-Pro.CA CDots at varying concentration. The inset shows the CD spectra for L-Pro.CA CDots at 5 mg mL^{-1} (C). Analysing signal sensitivity of L-Pro.CA CDots with different v/v% of free L-proline (D).

The spectral region that exhibits this phenomenon has been attributed to the $\pi \rightarrow \pi^*$ transition of CDots, which is potentially impacted by the augmented conjugation and aromaticity within the CDots. This, in turn, can result in an increased absorption of CDots, leading to scattering and a reduced signal-to-noise ratio during measurements. To avoid this, the optimum concentration for samples was adjusted to 1 mg mL^{-1} for all CD measurements. Following this observation, L-Pro.CA CDots were spiked with increasing concentration of amino acid to analyse the sensitivity of the CD profile to the presence of potential unreacted free amino acids in the solution. As shown in Fig. 3D, by increasing the concentration of L-proline from 5% v/v to 20% v/v, a noticeable shift occurs in the center of the absorbance from ~205 nm for the L-Pro.CA CDots, without any additives, to ~190 nm when containing 20% v/v free L-proline. Additionally, the CD spectra undergo a transformation from a negative absorbance to a couplet, with a matching position to the CD profile of L-proline when analysed independently. These observations provide further confirmation that the majority of L-proline molecules were involved in the CDots reaction, either through polymerization with the core, or weak interactions and attachment to the surface. Consequently, the resulting CD signal originates mostly from CDots rather than from unattached or unreacted amino acids in the solution.

It is noteworthy to highlight that both L-proline and citric acid were subjected to individual microwave irradiation under identical conditions as the L-Pro.CA CDots (Fig. S1). Despite observing an unchanged circular dichroism profile for both L-proline and citric acid before and after irradiation, a crucial observation emerged: while citric acid led to the formation of CDots, employing solely L-proline as the precursor did not result in CDots formation (as illustrated in Fig. S1A and B). This absence of CDots formation can be attributed to the limited unattached or unreacted amino acids within the solution, but they also emphasize the crucial role of both precursors in the formation of chiral CDots. The changes to the structure of the CDots were also supported by XRD analysis (Fig. S2). The amorphous halo centered at ~17° 2θ shown in the XRD pattern of the CDots is attributed to the presence of carboxylic acid groups within L-proline.

Of particular significance is the apparent reduction in the signal intensity of the amino acid upon heating, potentially indicating the loss of specific chiral centers that might have contributed to the formation of chiral CDots when combined with citric acid. These observations not only reinforce the notion that the predominant source of the resulting CD signal is indeed the CDots themselves, rather than arising from the amorphous carbon as the result of thermal decomposition of precursors.[56–58] Furthermore, the thermal stability of L-pro.CA CDots was assessed using TGA. The TGA analysis not only contributes to understanding the properties of CDots but also opens up potential avenues for their utilization in asymmetric catalysis and other applications. As shown in Fig. S3, the weight loss profiles of TGA were observed with increasing temperature, demonstrating that the chiral CDots consist of numerous functional groups and structures, as evidenced by the multi-step weight loss. The primary loss of mass in the temperature range of 30–160 °C can be attributed to the elimination of residual moisture and solvent adsorbed on the surface after the process of synthesis and purification. This is followed by greater weight losses occurring between approximately 180–500 °C, which are associated with the decomposition of various functional groups on the surface. Typically, functional groups containing oxygen and nitrogen undergo decomposition in this temperature range. Specifically, oxygen-containing functional groups, such as carboxyl, lactone, and anhydride, decompose at temperatures of less than 500 °C, resulting in the release of CO_2.[59] Furthermore, at temperatures exceeding 500 °C, the decomposition of phenols, ethers, and carbonyls occurs, which leads to the release of CO. The derivative curve revealed an oxidation temperature of approximately 27 °C, signifying the thermal stability of the chiral CDots. The TGA profile and stability of the L-pro.CA CDots are similar to those of CDots with similar compositions reported in prior studies.[28,60]

Antibacterial activity of chiral CDots

Proline is a component of many cell-penetrating antimicrobial peptides, helping shape their secondary structures[61,62] The chirality of proline-based CDots could thus be important in their penetration into the bacterial membrane, and therefore any potential antimicrobial activity. To assess this assumption, CDots were synthesized from both enantiomers of proline. As expected, the D-Pro.CA CDots have the opposite Cotton effect (Fig. 4A). Given the well-established impact of temperature on the chiral signal, we expected that elevating the temperature beyond 200 °C could lead to the breakdown of the chiral centers responsible for generating the signal observed in circular dichroism spectroscopy. Indeed, L-Pro.CA CDots synthesized using the same procedure but at 205 °C displayed similar spectra to DL-Pro.CA CDots made at 163 °C (Fig. 4A).

Following the synthesis of CDots, the MIC of the chiral precursors (L- and D-proline), both D- and L-Pro.CA CDots, and DL-Pro.CA CDots (racemic mixture) were assessed (Fig. 4B). The chiral precursors exhibited no antibacterial activity at the concentrations tested. This is not unexpected, as free proline is an osmoprotectant that has not been linked to growth inhibition.[63] Meanwhile, all three proline-based CDots showed weak activity. No discernible differences were observed between the D- and L-Pro.CA CDots prepared at 163 °C, suggesting an absence of stereospecific interactions between the CDots and their bacterial targets. Consistent with this hypothesis, the racemic DL-Pro.CA CDots displayed similar MIC values to those of the enantiopure CDots.

Surprisingly, nearly all bacterial strains were more sensitive to 163 °C CDots than those produced at 205 °C (Fig. 4B). This suggests that the chiral nature of the CDots, but not their specific chirality, may be important for antimicrobial activity. The microwave heating process may also break down or displace the constituent groups and structural features responsible for the antibacterial activity of the dots, interfering with activity against Gram-positive and Gram-negative bacteria.

To better understand how CDots inhibit bacterial growth, time-kill assays were performed. This assay involves exposing

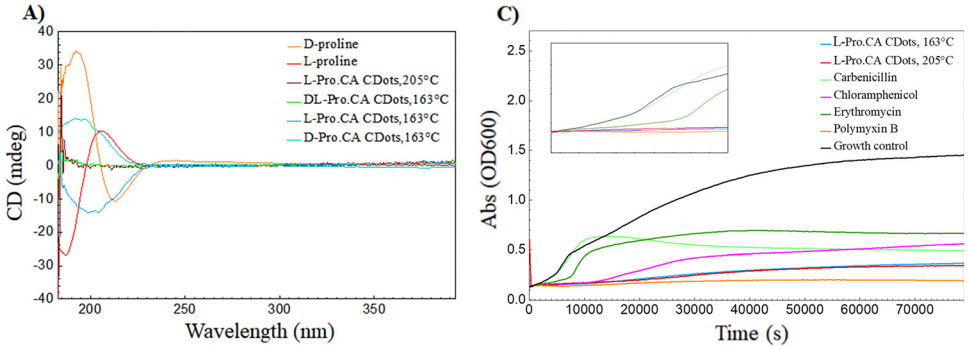

B)

Bacterial Strains Gram (+/-)	L-Pro.CDots 163 °C	L-Pro.CDots 205 °C	D-Pro.CDots 163 °C	DL-Pro.CDots 163 °C
	MIC (mg/mL)			
E. coli ATCC 25922 (−)	4	8	4	4
B. subtilis ATCC 6051 (+)	2	4	2	2
S. aureus ATCC 29213 (+)	2	4	2	2
P. aeruginosa CANWARD 113951 (−)	4	4	4	4
S. aureus CANWARD 115852 (+)	2	8	2	2

Fig. 4 CD spectra of chiral precursors and the corresponding chiral CDots used in bacterial studies, showcasing opposite cotton effects (A). MIC values of CDots against several bacterial strains (B). Time-kill assay of chiral and non-chiral CDots prepared at 163 °C and 205 °C, respectively (C). Precursors L-proline and D-proline did not show antibacterial activity in the ranges tested (MIC ≥16 mg mL^{-1}).

bacterial cultures to different concentrations of the antimicrobial agents and measuring the optical density over time. The concentrations used in the time-kill graph are as follows: CDots at 32 mg mL^{-1}, carbenicillin and polymyxin B at 8 μg mL^{-1} each, chloramphenicol at 4 μg mL^{-1}, and erythromycin at 64 μg mL^{-1}. The results of the assay can be used to determine whether a given antimicrobial exhibits bactericidal or bacteriostatic activity, as well as hinting to its mechanism of action. Based on the data presented in the growth curves in Fig. 4C, it appears that the mechanism of action for both chiral and non-chiral CDots is more similar to that of polymyxin B but less aggressive, as they seem to cause a rapid decline in bacterial growth. Polymyxin B is a polypeptide antibiotic that primarily targets the bacterial cell membrane, depolarizing the inner membrane of Gram-negative bacteria, dispersing the proton motive force and ultimately lysing the cell. The mechanism of action of CDs, including amino acid-doped CDs, has been predominantly attributed to an increased reactive oxygen species (ROS) generation leading to oxidative stress, and subsequent disruption of cell envelope integrity (cell wall/membrane damage).[64–67] These mechanisms are consistent with the rapid growth inhibition dynamics observed in our time-kill study. Therefore, the most likely mechanism of action of the CDots is membrane disruption.

Conclusions

In this study, we were able to successfully transfer the chiral properties of L-/D-proline to CDots and utilized RSM-BBD to study and optimize the reaction conditions that leads to preserving the maximum residual chiral signal of proline on the surface of CDots. Based on the optimization results, the second-order polynomial model revealed that the reaction temperature had the most significant impact on the magnitude of chiral response for CDots, while the molar ratio of precursors and exposure time exerted secondary effects. Furthermore, noteworthy interactions were observed between time and molar ratio, as well as time and temperature, playing a crucial role in shaping the chiral response on the surface of CDots. It is important to highlight that these interactions could not have been effectively explored using conventional one-factor-at-a-time approaches. As for their antibacterial properties, all three CDots prepared at 163 °C showed weak activity, which was not present when the CDots were prepared at 205 °C. Combined with the time-kill assay, this suggests a possible correlation between Pro.CA CDot structure and interactions with the bacterial membrane. Overall, this study provides valuable insights into the potential applications of chiral CDots and highlights the importance of considering the stereochemistry of active compounds when designing novel materials with enhanced properties.

Author contributions

Conceptualization, Arezoo Setayesh; formal analysis, Arezoo Setayesh and Laura Domínguez Mercado; methodology, Arezoo Setayesh; investigation, Arezoo Setayesh and Laura Domínguez Mercado; visualization, Arezoo Setayesh; validation, Arezoo Setayesh, Adryanne Clermont-Paquette; writing – original draft, Arezoo Setayesh; writing – review & editing, Arezoo Setayesh, Laura Domínguez Mercado, Adryanne Clermont-Paquette, Brandon L.

Findlay and Rafik Naccache; supervision, Brandon L. Findlay and Rafik Naccache; funding acquisition, Rafik Naccache.

Conflicts of interest

There are no conflicts to declare.

Data availability

The authors confirm that the data supporting the findings of this manuscript are available within the article and its supplementary information (SI). The supplementary information file contains tables for the experimental matrix used for the RSA, statistical analysis, circular dichorism, XRD and TGA analyses. See DOI: https://doi.org/10.1039/d5nj04463d.

Acknowledgements

The authors extend their gratitude to the funding sources that provided essential financial support for this research. RN acknowledges NSERC through the Discovery Grant program and FRQNT Equipe program for funding support. LD acknowledges FRQNT (B1X) and FRQS (Bourses de doctorat en recherche) for the support of this work. Additionally, RN appreciates the financial support received from Concordia University through the university Research Chair Program. RN also acknowledges support from the Quebec Centre for Advanced Materials. The TEM work was conducted at the Centre (CM)2 at McGill University, with valuable assistance provided by Ms Mohini Ramkaran.

Notes and references

1 J. George, S. Kar, E. S. Anupriya, S. M. Somasundaran, A. D. Das, C. Sissa, A. Painelli and K. George Thomas, *ACS Nano*, 2019, **13**, 4392–4401.
2 E. Vinegrad, U. Hananel, G. Markovich and O. Cheshnovsky, *ACS Nano*, 2019, **13**, 601–608.
3 M. V. Mukhina, V. G. Maslov, A. V. Baranov, A. V. Fedorov, A. O. Orlova, F. Purcell-Milton, J. Govan and Y. K. Gun'Ko, *Nano Lett.*, 2015, **15**, 2844–2851.
4 X. Wang, K. R. Deng, J. Wu, Y. Ma, X. Du, M. Zhang, H. Huang, Y. Liu and Z. Kang, *ACS Appl. Nano Mater.*, 2022, **5**, 16812–16820.
5 H. Wang, J. Qian, J. Gu, W. Yan and J. Zhang, *Biochem. Biophys. Res. Commun.*, 2019, **512**, 505–510.
6 J. Garciá-Guirado, M. Svedendahl, J. Puigdollers and R. Quidant, *Nano Lett.*, 2018, **18**, 6279–6285.
7 J. Cai, C. Hao, M. Sun, W. Ma, C. Xu and H. Kuang, *Small*, 2018, **14**(13), 1703931.
8 V. Kitaev, *J. Mater. Chem.*, 2008, **18**, 4745–4749.
9 X. Xu, R. Ray, Y. Gu, H. J. Ploehn, L. Gearheart, K. Raker and W. A. Scrivens, *J. Am. Chem. Soc.*, 2004, **126**, 12736–12737.
10 Z. Zhao, L. Tan, T.-B. Lv, J.-J. Zhang, K.-M. Liao, H.-Y. Wang, Z. Zeng, S. Deng and G.-P. Dai, *ACS Appl. Nano Mater.*, 2024, **7**, 13736–13744.
11 Z. Liu, L. Tan, P.-P. Hou, X.-J. Jin, M.-C. Li, Q.-Y. Zhou, P. Liao, Z. Zeng, S. Deng and G.-P. Dai, *Opt. Mater.*, 2022, **127**, 112368.
12 N. Xie, L. Tan, H.-F. Li, H.-Y. Hu, C. Wang, M. Pan and F. Wu, *et al.*, *J. Lumin.*, 2020, **219**, 116827.
13 W. Ma, B. Wang, Y. Yang and J. Li, *Chin. Chem. Lett.*, 2021, **32**, 3916–3920.
14 B. Wang, H. Cai, G. I. N. Waterhouse, X. Qu, B. Yang and S. Lu, John Wiley and Sons Inc, 2022, preprint, DOI: 10.1002/smsc.202200012.
15 G. Getachew, C. Korupalli, A. S. Rasal and J. Y. Chang, *Composites, Part B*, 2021, **226**, 109364.
16 A. Kaminari, E. Nikoli, A. Athanasopoulos, E. Sakellis, Z. Sideratou and D. Tsiourvas, *Pharmaceuticals*, 2021, **14**(9), 932.
17 L. Li, Q. Zhang, J. Li, Y. Tian, Y. Kang, G. Ren, W. Liu, H. Wang, B. Wang, L. Yan, L. Guo and H. Diao, *ACS Appl. Bio Mater.*, 2021, **4**, 7280–7289.
18 X. Dong, W. Liang, M. J. Meziani, Y. P. Sun and L. Yang, Ivyspring International Publisher, 2020, preprint, DOI: 10.7150/thno.39863.
19 D. Zhao, X. Liu, R. Zhang, X. Huang and X. Xiao, *New J. Chem.*, 2021, **45**, 1010–1019.
20 Y. Zhang, L. Hu, Y. Sun, C. Zhu, R. Li, N. Liu, H. Huang, Y. Liu, C. Huang and Z. Kang, *RSC Adv.*, 2016, **6**, 59956–59960.
21 S. Liu, Y. He, Y. Liu, S. Wang, Y. Jian, B. Li and C. Xu, *Chem. Commun.*, 2021, **57**, 3680–3683.
22 M. Zhang, W. Zhang, X. Fan, Y. Ma, H. Huang, X. Wang, Y. Liu, H. Lin, Y. Li, H. Tian, M. Shao and Z. Kang, *Nano Lett.*, 2022, **22**, 7203–7211.
23 P. Hou, T. Yang, H. Liu, Y. F. Li and C. Z. Huang, *Nanoscale*, 2017, **9**, 17334–17341.
24 A. C. P. Afonso, A. S. Correia, D. Duarte, A. T. S. C. Brandão, M. D. V. M. de Yuso, J. Jiménez-Jiménez, N. Vale, C. M. Pereira, M. Algarra and L. Pinto da Silva, *Chemosensors*, 2021, **9**(8), 191.
25 Q. Q. Zhang, T. Yang, R. S. Li, H. Y. Zou, Y. F. Li, J. Guo, X. D. Liu and C. Z. Huang, *Nanoscale*, 2018, **10**, 14705–14711.
26 X.-J. Jin, L. Tan, Z.-Q. Zhao, M.-C. Li, Q.-Y. Zhou, J.-J. Zhang and T.-B. Lv, *et al.*, *New J. Chem.*, 2023, **47**, 2221–2229.
27 F. Li, S. Li, X. Guo, Y. Dong, C. Yao, Y. Liu, Y. Song, X. Tan, L. Gao and D. Yang, *Angew. Chem., Int. Ed.*, 2020, **59**, 11087–11092.
28 E. Arad, S. K. Bhunia, J. Jopp, S. Kolusheva, H. Rapaport and R. Jelinek, *Adv. Ther.*, 2018, **1**(4), 1800006.
29 F. Victoria, J. Manioudakis, L. Zaroubi, B. Findlay and R. Naccache, *RSC Adv.*, 2020, **10**, 32202–32210.
30 F. Li, Y. Li, X. Yang, X. Han, Y. Jiao, T. Wei, D. Yang, H. Xu and G. Nie, *Angew. Chem.*, 2018, **130**, 2401–2406.
31 L. Zhou, D. Zheng, B. Wu, Y. Zhu and L. Zhu, *ACS Appl. Nano Mater.*, 2020, **3**, 946–952.
32 R. Malishev, E. Arad, S. K. Bhunia, S. Shaham-Niv, S. Kolusheva, E. Gazit and R. Jelinek, *Chem. Commun.*, 2018, **54**, 7762–7765.
33 M. J. Deka and D. Chowdhury, *RSC Adv.*, 2017, **7**, 53057–53063.
34 M. Zhang, Y. Ma, H. Wang, B. Wang, Y. Zhou, Y. Liu, M. Shao, H. Huang, F. Lu and Z. Kang, *ACS Appl. Mater. Interfaces*, 2021, **13**, 5877–5886.

35 Y. Wei, L. Chen, J. Wang, X. Liu, Y. Yang and S. Yu, *RSC Adv.*, 2019, **9**, 3208–3214.
36 F. Arshad and M. P. Sk, *New J. Chem.*, 2019, **43**, 13240–13248.
37 G. Wu, F. W. Bazer, R. C. Burghardt, G. A. Johnson, S. W. Kim, D. A. Knabe, P. Li, X. Li, J. R. McKnight, M. C. Satterfield and T. E. Spencer, *Amino Acids*, 2011, **40**(4), 1053–1063.
38 M. Mardirossian, R. Sola, B. Beckert, D. W. P. Collis, A. Di Stasi, F. Armas, K. Hilpert, D. N. Wilson and M. Scocchi, *ChemMedChem*, 2019, **14**, 2025–2033.
39 R. N. Roy, I. B. Lomakin, M. G. Gagnon and T. A. Steitz, *Nat. Struct. Mol. Biol.*, 2015, **22**, 466–469.
40 M. G. Gagnon, R. N. Roy, I. B. Lomakin, T. Florin, A. S. Mankin and T. A. Steitz, *Nucleic Acids Res.*, 2016, **44**, 2439–2450.
41 L. Otvos Jr., *Cell. Mol. Life Sci.*, 2002, **59**(7), 1138–1150.
42 I. Wiegand, K. Hilpert and R. E. W. Hancock, *Nat. Protoc.*, 2008, **3**, 163–175.
43 C. Xia, S. Zhu, T. Feng, M. Yang and B. Yang, John Wiley and Sons Inc., 2019, preprint, DOI: 10.1002/advs.201901316.
44 F. Wang, S. Pang, L. Wang, Q. Li, M. Kreiter and C. Y. Liu, *Chem. Mater.*, 2010, **22**, 4528–4530.
45 F. Wang, Z. Xie, H. Zhang, C. Y. Liu and Y. G. Zhang, *Adv. Funct. Mater.*, 2011, **21**, 1027–1031.
46 S. Sahu, B. Behera, T. K. Maiti and S. Mohapatra, *Chem. Commun.*, 2012, **48**, 8835–8837.
47 M. Lei, Y. Xie, L. Chen, X. Liu, Y. Yang, J. Zheng and Q. Li, *RSC Adv.*, 2022, **12**, 27431–27441.
48 Y. Zhang, Y. Wang, X. Feng, F. Zhang, Y. Yang and X. Liu, *Appl. Surf. Sci.*, 2016, **387**, 1236–1246.
49 S. Zhu, Q. Meng, L. Wang, J. Zhang, Y. Song, H. Jin, K. Zhang, H. Sun, H. Wang and B. Yang, *Angew. Chem., Int. Ed.*, 2013, **52**, 3953–3957.
50 S. S. Wee, Y. H. Ng and S. M. Ng, *Talanta*, 2013, **116**, 71–76.
51 J. R. Macairan, T. V. de Medeiros, M. Gazzetto, F. Yarur Villanueva, A. Cannizzo and R. Naccache, *J. Colloid Interface Sci.*, 2022, **606**, 67–76.
52 T. V. De Medeiros, J. Manioudakis, F. Noun, J. R. Macairan, F. Victoria and R. Naccache, *J. Mater. Chem., C*, 2019, **7**, 7175–7195.
53 S. N. Baker and G. A. Baker, *Angew. Chem., Int. Ed.*, 2010, **49**(38), 6726–6744.
54 G. Tong, J. Wang, R. Wang, X. Guo, L. He, F. Qiu, G. Wang, B. Zhu, X. Zhu and T. Liu, *J. Mater. Chem. B*, 2015, **3**, 700–706.
55 K. L. Carlson, S. L. Lowe, M. R. Hoffmann and K. A. Thomasson, *J. Phys. Chem. A*, 2006, **110**, 1925–1933.
56 B. Zhang, J. Ren, X. Liu, Y. Guo, Y. Guo, G. Lu and Y. Wang, *Catal. Commun.*, 2010, **11**, 629–632.
57 J. Manioudakis, F. Victoria, C. A. Thompson, L. Brown, M. Movsum, R. Lucifero and R. Naccache, *J. Mater. Chem. C*, 2019, **7**, 853–862.
58 V. M. Naik, S. V. Bhosale and G. B. Kolekar, NLM (Medline), 2022, preprint, DOI: 10.1039/d1ay02105b.
59 L. Li, X. Yao, H. Li, Z. Liu, W. Ma and X. Liang, *J. Chem. Eng. Jpn.*, 2014, **47**, 21–27.
60 G. Filippini, F. Amato, C. Rosso, G. Ragazzon, A. Vega-Peñaloza, X. Companyó, L. Dell'Amico, M. Bonchio and M. Prato, *Chem*, 2020, **6**, 3022–3037.
61 M. Graf, M. Mardirossian, F. Nguyen, A. C. Seefeldt, G. Guichard, M. Scocchi, C. A. Innis and D. N. Wilson, Royal Society of Chemistry, 2017, preprint, DOI: 10.1039/c7np00020k.
62 F. Guida, M. Benincasa, S. Zahariev, M. Scocchi, F. Berti, R. Gennaro and A. Tossi, *J. Med. Chem.*, 2015, **58**, 1195–1204.
63 S. Cayley, B. A. Lewis and M. T. Record Jr., *J. Bacteriol.*, 1992, **174**, 1586–1595.
64 Y. Li, W. Zhang, J. Niu and Y. Chen, *ACS Nano*, 2012, **6**, 5164–5173.
65 X. Hao, L. Huang, C. Zhao, S. Chen, W. Lin, Y. Lin and L. Zhang, *et al.*, *Mater. Sci. Eng., C*, 2021, **123**, 111971.
66 Y. Wu, C. Li, H. C. van der Mei, H. J. Busscher and Y. Ren, *Antibiotics*, 2021, **10**, 623.
67 M. Yu, P. Li, J. Li, X. Chen, Z. Hu, Y. Wang and J. Zeng, *et al.*, *Adv. Healthcare Mater.*, 2025, **14**, 2403201.

